Exciton dynamics in $In_xGa_{1-x}As/GaAs$ quantum-well heterostructures: Competition between capture and thermal emission

G. Bacher, C. Hartmann, and H. Schweizer
4. Physikalisches Institut, Universität Stuttgart, Pfaffenwaldring 57, D-7000 Stuttgart 80, Federal Republic of Germany

T. Held and G. Mahler
Institut für Theoretische Physik, Universität Stuttgart, Pfaffenwaldring 57, D-7000 Stuttgart 80, Federal Republic of Germany

H. Nickel
Deutsche Bundespost TELEKOM, Forschungsinstitut, P.O. Box 100003, D-6100 Darmstadt, Federal Republic of Germany
(Received 19 October 1992)

In a carefully selected set of strained $In_xGa_{1-x}As/GaAs$ quantum-well structures, we have studied experimentally and theoretically the competition between carrier collection from the GaAs barrier into the quantum wells and the inverse process, the thermal activated emission out of the wells into the barrier. Analyzing the temperature dependence of time-integrated photoluminescence measurements, we found excitons or electron-hole pairs to be emitted out of the well. A different sample geometry is used to demonstrate the importance of the barrier properties in the equilibrium of capture and thermal emission. Time-resolved experiments allow the determination of the typical time constants, namely the radiative and the nonradiative recombination lifetime as well as the emission time. A hydrodynamic model, including the diffusion in the barrier and the carrier capture and emission via LO phonons, was developed for a quantitative description of our experiments. With use of the experimental time constants, an excellent agreement between the time-integrated experiments and theory was found, giving evidence of the applicability of our model.

I. INTRODUCTION

Due to the increasing application potential of semiconductor quantum-well structures for the development of heterostructure lasers as well as high-speed electrical devices, the efficiency of the carrier collection into the active region, i.e., the quantum well, is of considerable interest.[1] Various experimental work using time-integrated[2–5] and time-resolved[6–12] photoluminescence (PL) spectroscopy, as well as a couple of theoretical[6,13–19] works, has been done for a quantitative understanding of the capture process. The capture process can be described by the energy loss of the specific carrier due to the emission of optical phonons.[13–15,17,18] While the theoretical results[13,15,18] yield capture times between several ps and ns, depending on sample geometry, the time constants found experimentally[8–11] using time-resolved photoluminescence spectroscopy are of the order of several ps. However, the carrier collection into the quantum well is not only determined by the quantum-mechanical capture time, but also by the carrier transport in the barrier.[5–9,15,16] The transport time can be reduced drastically by using graded index confinement layers.[5,8,12]

For practical applications, a good laser performance at room temperature is necessary. However, it has been found that photoluminescence efficiency is reduced with increasing temperature in most of the structures investigated due to nonradiative carrier loss. An important carrier-loss process, the thermal emission of the carriers out of the quantum well into the barrier, was recently found.[20–24] This process is especially important in shallow quantum wells, occurring also in high-quality samples and reducing the carrier density in the quantum well with increasing temperature. Thus, the carrier distribution between the active region (the quantum well) and the confining layers (the barriers) is controlled by both the collection efficiency by the quantum well and the inverse process, the thermal emission of the carriers into the barrier.

In a set of specially designed $In_xGa_{1-x}As/GaAs/Al_yGa_{1-y}As$ quantum-well heterostructures, we have systematically investigated the competition between the carrier collection into the quantum well and the thermal emission out of the wells using time-integrated and time-resolved PL spectroscopy. The temperature dependence of the PL intensity of the quantum-well emission reveals a lot of information about the mechanism of the thermal emission process. Varying the barrier geometry allows a detailed discussion of the equilibrium between the capture and emission of photoexcited carriers. For the description of our experimental results with a hydrodynamic model, an accurate determination of the characteristic time constants was performed using time-resolved PL spectroscopy. Including the experimental parameters in the theoretical model, a complete description of the temperature dependence of the PL intensity for different sample geometrys is achieved, emphasizing the importance of LO-phonon scattering for the capture and for the thermal-activated emission process. The interaction between neighboring quantum wells as well as the influence of nonradiative processes at the

 ©1993 The American Physical Society

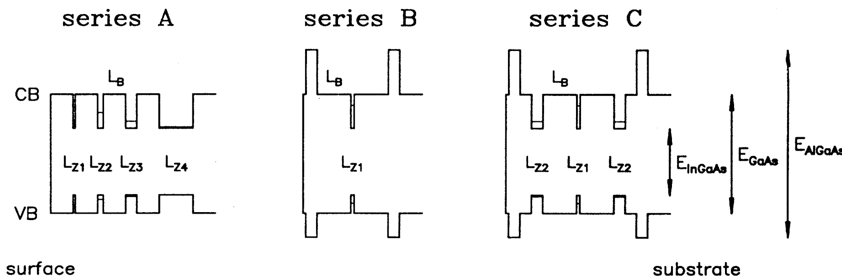

FIG. 1. Schematic description of the designed sample structures used in our experiments. Depicted is the energy versus the growth direction z. The sample parameters are discussed in the text.

sample surface or in the substrate and at the $GaAs/Al_yGa_{1-y}As$ heterointerface, respectively, is demonstrated and quantitatively explained. Previous results of our experiments have already been published.[20]

We have organized the paper as follows. In Sec. II, the sample structures are explained with respect to their function and time-integrated experiments are presented, demonstrating the influence of the temperature on the equilibrium between capture and emission. The results deduced from time-resolved experiments are discussed in Sec. III. In Sec. IV, the hydrodynamic model evaluated for the description of the experimental data is introduced and in Sec. V we compare and discuss the experimental and the theoretical results. A summary concludes our paper.

II. EXPERIMENT A: SAMPLE CHARACTERIZATION AND TIME-INTEGRATED PHOTOLUMINESCENCE SPECTROSCOPY

For a detailed understanding of the competition between carrier capture and thermal emission, we have designed and investigated shallow $In_xGa_{1-x}As/GaAs/Al_yGa_{1-y}As$ heterostructures. Epitaxially, a wide range of structural parameters has been varied to obtain full information of the exciton dynamics especially of the size-dependent capture and emission process, respectively, as well as the carrier diffusion in the barrier and the influence of the surfaces and interfaces. The geometry of the heterostructures under investigation is schematically presented in Fig. 1. The samples were grown on undoped (100)-oriented GaAs substrates in a Varian molecular-beam-epitaxy 360 system with rotating substrate holder. Details of the growth procedure are given elsewhere.[25]

There are three samples of series A with different In content x ($x=0.06$, 0.12, and 0.2, respectively), each containing 4 (for $x \leq 0.12$) or 3 (for $x=0.2$) quantum wells with different well width L_z ($L_z=2$, 5, 10, and 30 nm for $x \leq 0.12$; $L_z=2$, 5, and 10 nm for $x=0.2$) separated by a 200-nm GaAs barrier. No additional $Al_yGa_{1-y}As$ confining layer is included. This structure with various shallow quantum wells is used to perform a detailed investigation of the influence of quantum-well geometry (well width and confinement energy) on the carrier dynamics. All the samples of series B and C contain one quantum well with $x=0.2$ and $L_z=3$ nm. This quantum well is symmetrically cladded by a GaAs barrier of variable thickness ($L_B=60$, 300, and 1200 nm, respectively). Whereas in series B, the $GaAs/In_{0.2}Ga_{0.8}As/GaAs$ structure is directly enclosed by a $Al_{0.35}Ga_{0.65}As$ cladding layer, the samples of series C additionally contain two quantum wells with $L_z=10$ nm, distributed symmetrically to the central $L_z=3$ nm well in the distance L_B. The different barrier geometry available allows a justification of the hydrodynamic model with respect to the carrier dynamics in the barrier, e.g., the carrier transport.

To demonstrate the influence of sample geometry on the PL emission characteristics, we present in Fig. 2 a

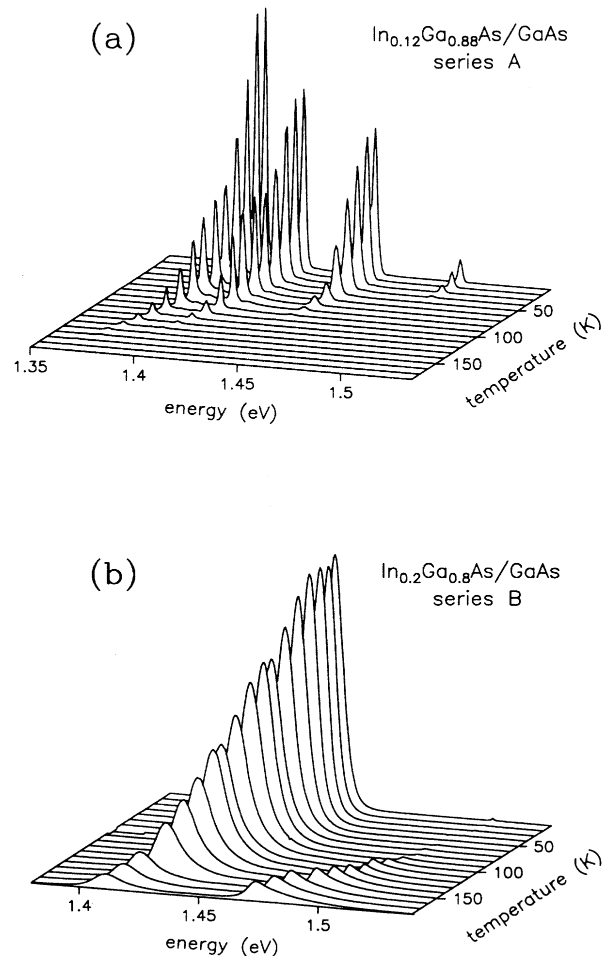

FIG. 2. Comparison between the temperature evolution of the PL spectrum of a sample of series A ($x=0.12$; $L_z=2$, 5, 10, and 30 nm, respectively) and a sample of series B ($x=0.2$; $L_z=3$ nm; $L_B=1200$ nm).

comparison of the temperature dependence between the PL spectra of two different samples. The samples were excited nonresonantly in the barrier using a cw dye laser and a cw Ti-sapphire laser, respectively. In the $In_{0.12}Ga_{0.88}As$/GaAs sample of series A [Fig. 2(a)], we observe an efficient carrier capture of the photoexcited carriers at $T=10$ K, causing a PL spectrum dominated by the emission of the quantum wells ($L_z=2$, 5, 10, and 30 nm, respectively). Increasing the temperature yields a successive reduction of the luminescence intensity. It is a striking feature that first the PL intensity of the smallest quantum well is quenched, while the PL intensity of the wider wells can still be detected at higher temperatures, depending on well width. At room temperature, the total PL efficiency is very small. Negligible luminescence from the GaAs barrier is observed in the whole temperature range under investigation. On the other hand, the PL spectra of a sample of series B [$L_z=3$ nm, $L_B=1200$ nm; see Fig. 2(b)] reveal a different behavior. Increasing the bath temperature changes the ratio between quantum well and barrier luminescence and at $T>160$ K, the GaAs luminescence even dominates the spectrum. The total intensity of this sample is only reduced by one order of magnitude at room temperature compared to the low-temperature intensity. From these results, we conclude that the equilibrium between the carrier capture into the quantum well and the thermal-activated carrier emission out of the well changes with temperature, causing an increasing barrier population at higher temperatures.

This comparison gives evidence of the importance of both the quantum well and the barrier geometry for the behavior of the temperature dependence of the radiative efficiency of the quantum well and the barrier, respectively. Thus, the inclusion of an additional $Al_xGa_{1-x}As$ cladding layer in the sample of series B prevents the carrier diffusion to the surface or into the substrate and therefore suppresses nonradiative recombination at the interfaces.

From an experimental point of view, it is not clear up to now whether only the carrier capture efficiency is reduced with increasing temperature or an efficient emission of the carriers out of the quantum well into the barrier can occur. Hence, we have performed photoluminescence excitation (PLE) spectroscopy experiments (Fig. 3). In contrast to "normal" PLE, where the energy of the exciting laser is higher than the detection energy, we have detected the GaAs barrier luminescence and generated carriers tuning the laser between resonant (below the barrier) and nonresonant (above the barrier) excitation. For a resonant excitation of the $In_{0.2}Ga_{0.8}As$ quantum well, we found a distinct emission of the GaAs barrier, indicating an efficient transfer of optically generated carriers from the low-energy quantum well to the barrier at higher energy.[26] To investigate the influence of the excitation energy on the carrier distribution, we have measured the PL spectrum at $T=170$ K by changing the wavelength of the exciting laser from resonant excitation in the quantum well to nonresonant excitation in the barrier. If the excitation power was adjusted carefully to obtain a constant carrier density in the quantum well, no significant change of the ratio between the quantum well and the barrier luminescence was found. From this result, we conclude that the equilibrium between the carrier density in the well and in the barrier in this high-temperature regime is established very fast with respect to the recombination lifetime (see Sec. III).

For a quantitative determination of the activation energy of the thermal emission process, the PL intensity is depicted versus temperature in an Arrhenius plot in Fig. 4 for a set of different quantum wells. In all the samples, the PL intensity is nearly constant at low temperatures up to a characteristic "drop" temperature T_D. Then the

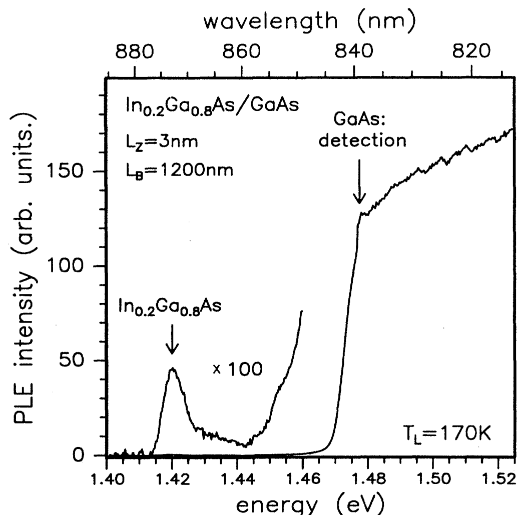

FIG. 3. PLE spectrum in a sample of series B ($x=0.2$; $L_z=3$ nm; $L_B=1200$ nm). The emission of the GaAs barrier was detected, while the excitation energy was tuned between the energy level of the quantum well and the nonresonant excitation in the barrier. The bath temperature of 170 K causes an efficient thermal emission into the barrier of the carriers created in the well.

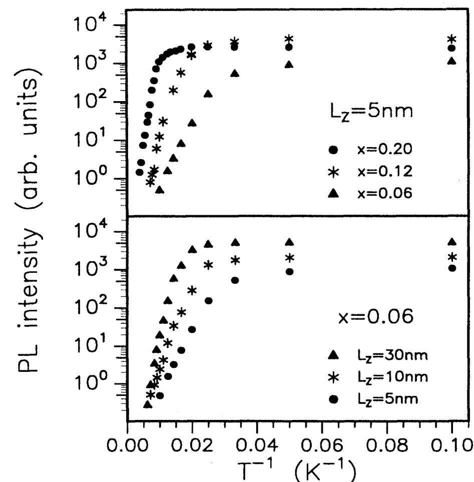

FIG. 4. PL intensity vs temperature in an Arrhenius plot for different samples. Compare the dependence of the thermal emission process on In content x (for $L_z=5$ nm; top) and on well width L_z (for $x=0.06$; bottom).

intensity is quenched drastically for a further increase in temperature. The onset of this intensity drop as well as the characteristic activation energy E_A describing the intensity reduction depends on In content x (see Fig. 4, top) and on well width L_z (see Fig. 4, bottom). The shallower the quantum well, the smaller the activation energy E_A and the characteristic temperature T_D. Note, that the quenching of the PL intensity starts at temperatures $T \ll E_A/k$ due to the change in the density of states between the quantum well and the barrier.

A determination of the activation energy from the slope of the temperature dependence of the PL intensity reveals a rather interesting result (see Fig. 5): Within experimental error ($\pm 10\%$), the activation energy E_A corresponds to the difference between the quantum well and the barrier emission (here defined as total confinement energy ΔE), i.e., the sum of the electron and the hole potential depth (solid line in Fig. 5). Excitons or electron-hole pairs are emitted into the barrier. This is in agreement with an estimation of the arising electric field if only one type of carrier (electrons or holes) would be emitted into the barrier. The electric field would lower the barrier and immediately cause an emission of the carriers with opposite charge to establish an equilibrium.[23] As pointed out by Michler *et al.*,[23] an activation energy E_A which is equal to $\Delta E/2$ (dotted line) can be expected in the low injection case, where the background doping level is higher than the optically generated carrier density. The result $E_A = \Delta E$ thus demonstrates the high quality of the samples investigated. Because of our experimental error and because of the small difference in the exciton binding energy in the quantum well and in the barrier, we cannot distinguish whether excitons or electron-hole pairs are emitted into the barrier. However, for the low excitation conditions used in our experiments, we observe mainly excitonic emission. Thus, the hydrodynamic model introduced in Sec. IV takes excitons as the dominating particles.

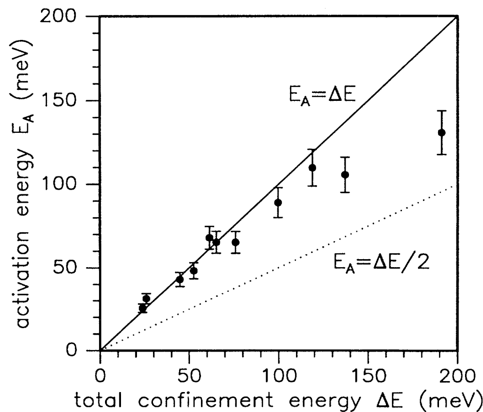

FIG. 5. Activation energy E_A as deduced from the Arrhenius plot vs the total confinement energy ΔE, which is given by the difference between the exciton emission of the quantum well and the barrier. The solid line and the dotted line illustrate the expected connection in the case of high-injection and low-injection conditions, respectively.

For larger confinement energies, especially in the wider wells of the sample with an In content of $x = 0.2$, we observe a deviation from the linear connection between E_A and ΔE. This can be due to additional nonradiative processes occurring at higher temperatures and thus modifying especially the activation energy in deeper quantum wells. On the other hand, the emission process is responsible for a thermal coupling of the different quantum wells via transport in the barrier. As already discussed in our previous paper (see the inset of Fig. 2 of Ref. 20), this coupling, which is most effective in the sample with $x = 0.2$, modifies the activation energy E_A. The carriers thermally emitted out of shallow quantum wells can be captured in the neighboring wells with higher barriers, increasing the PL intensity of the deeper wells.

Whereas the activation energy E_A is mainly controlled by the depth of the potential well, we will discuss in the following the influence of the barrier geometry on the emission process. In Fig. 6, we have compared the evolution of the PL intensity of a 3-nm quantum well ($x = 0.2$) with temperature for two samples with different geometry. While the sample of series B consists only of this center well embedded between two GaAs barriers ($L_B = 1200$ nm), the other sample (series C) contains two additional quantum wells with $L_z = 10$ nm in a distance of $L_B = 1200$ nm to the center well (see Fig. 1), acting as "traps" for the carriers thermally emitted out of the quantum well with $L_z = 3$ nm. This incoherent coupling between different quantum wells changes the characteristic temperature T_D, while the activation energy E_A remains constant. A non-Arrhenius behavior occurs at higher temperatures in the sample of series C (another increase of the PL intensity with temperature is observed) due to the coupling between the 3- and 10-nm quantum wells in this sample. This will be discussed in more detail in Sec. V.

A comparison of samples of series B consisting of the same principal structure but with different barrier width L_B is illustrated in Fig. 7. For nonresonant excitation in the GaAs barrier, the ratio of the PL intensity of the barrier and the $In_{0.2}Ga_{0.8}As$ quantum well is depicted versus

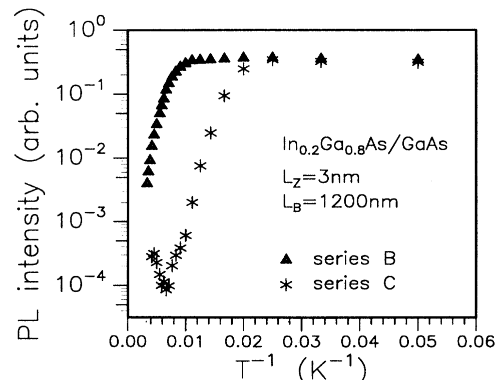

FIG. 6. PL intensity vs temperature in an Arrhenius plot for a quantum well with $L_z = 3$ nm and $x = 0.2$ embedded in a different sample geometry, demonstrating the influence of the complete sample structure on the thermal emission process.

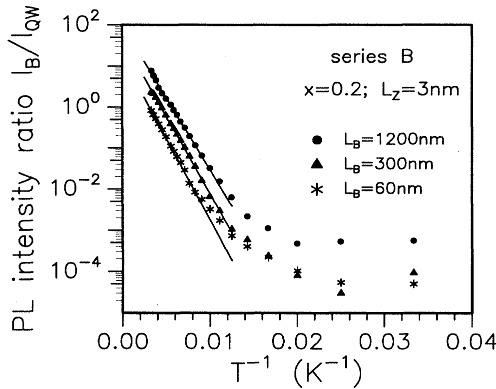

FIG. 7. Ratio of the barrier and the quantum-well emission vs temperature for different barrier geometries. The solid line according to $I_B/I_{QW}=C\exp(-E_A/kT)$ describes the experimental data for $T>100$ K. The parameter C depends on the barrier width L_B and is found to be 17, 47, and 100 for $L_B=60$, 300, and 1200 nm, respectively.

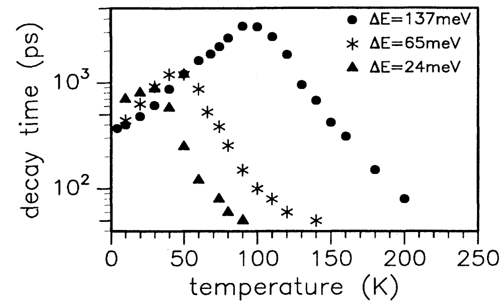

FIG. 8. PL decay time vs temperature for different confinement energies ΔE. All the time constants are taken from samples of series A.

$1/T$. At low temperatures, the PL spectrum of each sample is dominated by the light emission of the quantum well. With increasing temperature, the PL intensity of the barrier grows up while the intensity of the well is reduced. Hence, the ratio I_B/I_{QW} increases according to the activation energy E_A. This can be described by

$$\frac{I_B}{I_{QW}}=C\exp(-E_A/kT)\ , \tag{1}$$

where E_A is given by the potential height of the barrier and is therefore independent of the barrier width L_B. The factor C does not only include the geometrical ratio of the well width L_z and the barrier width L_B, but also the characteristic time constants, i.e., the recombination lifetimes of the barrier and the well, the emission time, and the overall collection time, including the transport to the well. The deviation between Eq. (1) and the experimental data demonstrate that at low temperatures the thermal equilibrium cannot be established within the excitonic lifetime because of the enhanced transport time in the barrier in this temperature regime. From this point of view, it is clear that a consistent theoretical description of our experiments must not only consider the quantum-well properties, but also the structure of the complete sample, including barrier geometry and additional layers as well as surface and interface properties.

III. EXPERIMENT B: TIME-RESOLVED EXPERIMENTS

For a quantitative description of the time-integrated PL measurements, an exact knowledge of the characteristic time constants, especially the exciton lifetime, is required. For that reason, we have performed time-resolved experiments. In the experimental setup, sample excitation was carried out using a cw-mode-locked Ar^+ laser followed by a synchronously pumped dye laser (DCM or Styryl 9, respectively; pulse width 10 ps). The PL signal was dispersed by a double monochromator and detected by a fast micro channel plate multiplier with $S1$ characteristic. The time resolution of the complete setup was about 50 ps.

First, we will discuss the modification of the temperature evolution of the exciton decay time in the quantum well due to the well and the barrier geometry, respectively. In Fig. 8 the decay time of the PL signal is depicted versus temperature for quantum wells with different confinement energies ΔE. At low temperatures, we find an increase of the decay time with temperature (up to around 3.5 ns) in qualitative agreement with the temperature dependence of excitonic recombination.[27,28] At a characteristic temperature, depending on ΔE, a strong reduction of the decay time is observed. This drop occurs at higher temperatures if L_z or x, which determine the total confinement energy, increases. As the experimental determined PL lifetime is composed of a radiative part, which should increase with temperature, and a nonradiative part, we relate the drop of the PL lifetime to an increasing influence of nonradiative carrier loss in the quantum well. Both the reduction of the PL intensity (Fig. 4) and the decrease of the PL decay time (Fig. 8) are obviously caused by the same process, namely, the thermal activation of the excitons into the barrier. Hence, at higher temperatures, the measured decay time is mainly determined by the thermal emission time.

To demonstrate the influence of the sample structure on the decay time, we have plotted in Fig. 9 a comparison between one sample of series B ($L_{z1}=3$ nm; $L_B=1200$ nm) and one sample of series C ($L_{z1}=3$ nm; $L_{z2}=10$ nm; $L_B=1200$ nm). The decay time of the well with $L_{z1}=3$ nm is depicted versus temperature. At $T\leq 40$ K, the decay time increases due to the increasing excitonic lifetime in both samples. However, further increasing the temperature reveals a drastic difference between these two samples. While the decay time in the sample of series B increases further up to 150 K and then saturates at a value of around 30 ns, the decay time of the sample of series C drops down to around 100 ps at $T=120$ K. This clearly demonstrates that the additional traps, i.e., the quantum wells with $L_z=10$ nm in the sample of series C, catch the carriers emitted out of the thin quantum well, reducing the effective decay time in the quantum well under investigation. On the other hand, in the sample of series B, the carriers can either recombine in the well or

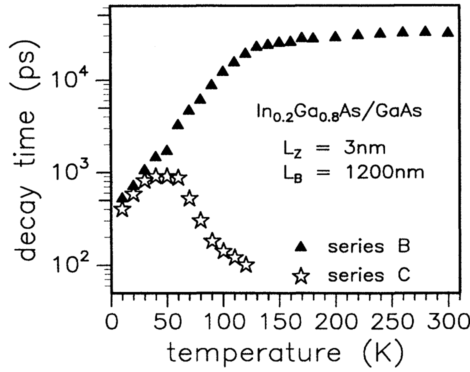

FIG. 9. Comparison between the decay time of a quantum well with $L_z = 3$ nm and $x = 0.2$ embedded in different sample structures as described in the text. The additional 10-nm quantum wells in series C reduce the time constant of the 3-nm quantum well under investigation drastically.

in the barrier and for a small nonradiative recombination rate, the time constant observed can become very long due to the increasing lifetime in the well and in the barrier with increasing temperature. The large value of the recombination lifetime at room temperature demonstrates the applicability of such heterostructures for the development of low-threshold semiconductor lasers.

From this point of view, we will shortly comment on the results depicted in Fig. 8. In all the quantum wells, the decay time is reduced at increasing temperature due to thermal emission. These samples of series A contain no additional $Al_yGa_{1-y}As$ confinement layer. Hence, the carriers thermally emitted out of the wells can reach the surface or the substrate and efficiently recombine nonradiatively. In conclusion, a fast nonradiative recombination channel in the barrier, i.e., additional quantum wells with larger confinement energy acting as additional traps or surfaces or to a smaller degree interfaces acting as nonradiative centers, catch the thermal emitted carriers and therefore reduce the measured decay time in the quantum well under investigation drastically with increasing temperature.

A separation of the radiative and the nonradiative recombination lifetime is possible under the assumption that the measured decay rate is given by the sum of the radiative and the nonradiative rate,[29]

$$\frac{1}{\tau(T)} = \frac{1}{\tau_{\mathrm{rad}}(T)} + \frac{1}{\tau_{\mathrm{nrad}}(T)} . \tag{2}$$

Hence, for the temperature-dependent PL intensity we can write

$$I(T) = I_0 \frac{\tau(T)}{\tau_{\mathrm{rad}}(T)} . \tag{3}$$

Because in all our samples the PL intensity for $T < T_D$ is nearly independent of temperature, we assume a purely radiative recombination at $T = 10$ K which yields $I_0 = I(10\ \mathrm{K})$. Then, we get for the radiative and the nonradiative recombination times,

$$\tau_{\mathrm{rad}}(T) = \frac{I(10\ \mathrm{K})}{I(T)} \tau(T) ,$$
$$\tau_{\mathrm{nrad}}(T) = \frac{I(10\ \mathrm{K})}{I(10\ \mathrm{K}) - I(T)} \tau(T) . \tag{4}$$

$I(T)$ and $\tau(T)$ were determined experimentally (see Figs. 4–9). According to Eqs. (2)–(4), a separation between the radiative and the nonradiative part of recombination can be performed as depicted in Fig. 10. On the left side, the time constants of a sample of series B are analyzed. Whereas the radiative lifetime increase with temperature, according to theory,[27,28] by controlling the experimental values up to $T \simeq 100$ K, we observe at higher temperatures mainly a temperature-independent nonradiative recombination time. From comparison with the temperature dependence of the PL intensity as presented in Fig. 6, we notice that the nonradiative recombination dominates at temperatures where an efficient thermal emission into the barrier is observed. It is obvious that the nonradiative recombination center is located in the barrier, possibly at the $GaAs/Al_yGa_{1-y}As$ heterointerface. We discuss this point in more detail in Sec. V. In the sample of series C (see the right-hand side of Fig. 10), the temperature dependence of the radiative recombination rate is, in principle, the same. However, the nonradiative lifetime decreases strongly with increasing temperature. In this sample, this time constant is given by the thermal emission time into the barrier followed by a fast capture of the emitted carriers into the neighboring 10-nm quantum wells. Thus, we conclude that the coupling of different wells via transport in the barrier drastically modifies the exciton dynamics. Using this method for all the quantum wells under investigation, we are able to

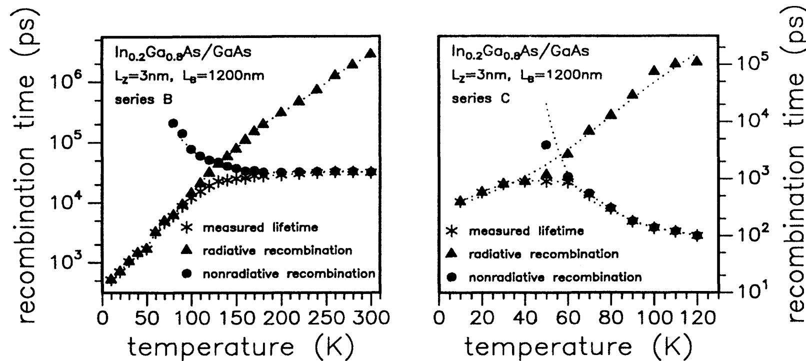

FIG. 10. Separation of the radiative and the nonradiative part of the recombination for a 3-nm $In_{0.2}Ga_{0.8}As/GaAs$ quantum well in a sample of series B ($L_B = 1200$ nm; to the left) and a sample of series C ($L_{z2} = 10$ nm and $L_B = 1200$ nm; to the right). The dotted lines are guides to the eye.

determine the radiative recombination lifetime in the wells, which are needed in the theoretical description of our experiments (see Secs. IV and V).

IV. THE HYDRODYNAMIC MODEL

The dynamics of electronic particles in a quantum well is not only determined by the emission into the barrier and the recombination in the well. A complete model must also take into account the dynamics in the barrier, i.e., the transport and the reflection, transmission, and capture of particles approaching the quantum well. The details of the model are given by the sample geometry and experimental scenario. A continuous-wave excitation at low energy reduces hot carrier effects compared to short-pulse excitation. Small laser power densities lead to carrier densities below the Mott density and thus to the formation of excitons. In our case, an analysis of the thermal behavior of the quantum-well luminescence also tells us that excitons are the dominating electronic particles. Therefore we take a set of continuity equations for the density of excitons in the bulk n^{3D} and in the quantum wells n_i^{2D} (where i is the number of the quantum well) and Fick's law for the particle current density j,

$$\frac{\partial n^{3D}}{\partial t}+\frac{\partial}{\partial z}j=g^{3D}e^{-\alpha^{3D}z}-\frac{n^{3D}}{\tau^{3D}} , \tag{5}$$

$$\frac{\partial n_i^{2D}}{\partial t}+j|_i^r-j|_i^l=g_i^{2D}e^{-\alpha_i^{2D}z}-\frac{n_i^{2D}}{\tau_i^{2D}} , \tag{6}$$

$$j=-D\frac{\partial n^{3D}}{\partial z} , \tag{7}$$

where $j|_i^l$ and $j|_i^r$ denote the particle current density at the left and at the right border of the quantum well i, D is the diffusion coefficient, and g, α, τ the generation rate, absorption coefficient, lifetime in the bulk [three dimensional (3D)] and quantum wells [two dimensional (2D)], respectively. The laser light is assumed to enter the sample at $z=0$.

To get boundary conditions for these equations we use a microscopic model[14,30] which has been successfully applied for the description of time-resolved experiments studying the vertical transport in $GaAs/Al_{0.5}Ga_{0.5}As$ heterostructures.[6] As mentioned before a particle approaching a quantum well may either be reflected, transmitted, or captured. This is illustrated schematically in Fig. 11. The sum of these three probabilities has to be equal to one, i.e., only two of them appear in the equations. Multiplied with a thermal velocity $v_{th}=\sqrt{k_BT/2\pi m^*}$ (T equals the particle temperature; m^* equals the effective mass) we get "interface velocities," in our case the transmission velocity s_i^t and the capture velocity s_i^c. The emission probability is expressed as an inverse time $1/\tau_i^{out}$. Thus we get

$$j|_i^l=n^{3D}|_i^l(s_i^t+s_i^c)-\frac{n_i^{2D}}{2\tau_i^{out}}-n^{3D}|_i^r s_i^t , \tag{8}$$

$$j|_i^r=-n^{3D}|_i^r(s_i^t+s_i^c)+\frac{n_i^{2D}}{2\tau_i^{out}}+n^{3D}|_i^l s_i^t . \tag{9}$$

The capture of a particle into the well and the emission out of the well is considered a scattering process with an optical phonon. For the exact formula of s_i^c and τ_i^{out} we refer[31] to Appendix A.

To complete the boundary conditions, the interfaces to the $Al_{0.35}Ga_{0.65}As$ cladding layers or the surface of the sample and the interface to the substrate, respectively, are treated as quantum wells with $s^t=0$. In the following, we call these planes of the sample simply "interfaces." The capture and emission at these interfaces are free eligible parameters. The whole set of equations is analytically solved under steady-state conditions as described in Appendix B.

By simulating the PL intensity at several temperatures, the importance of the interface parameters occurs: in Fig. 12 the calculations of the dynamics in a sample of series C with three different interfaces is shown. The strength of the reflection (or the capture, respectively) at the interfaces does not only influence the particle distribution in the quantum wells next to the $GaAs/Al_yGa_{1-y}As$ interfaces ($L_{z2}=10$ nm) but also in the central one ($L_{z1}=3$ nm) due to a strong coupling of the wells via transport.

In case of a completely absorbing $Al_yGa_{1-y}As$ barrier, we see that by increasing temperature first the excitons leave the narrow (and shallow) quantum well ($L_{z1}=3$ nm) and at higher temperatures the wider (and deeper) wells ($L_{z2}=10$ nm) are emptied. In the other extreme case, a completely reflecting barrier shows a rather different behavior: at lower temperature it is similar to the first case which means that all emitted excitons are mainly absorbed by the wide wells, but then the wide wells begin to emit excitons and the density in the narrow well increases again. This emission of the wide wells is not very effective because the excitons are sent into the direction of the $Al_yGa_{1-y}As$-barrier return and are reabsorbed. If the barrier is a synthesis of these extreme cases it is obvious that the density in the wide wells can decrease and that the reincrease of the density in the narrow well is not so emphasized. Nevertheless, we can draw conclusions

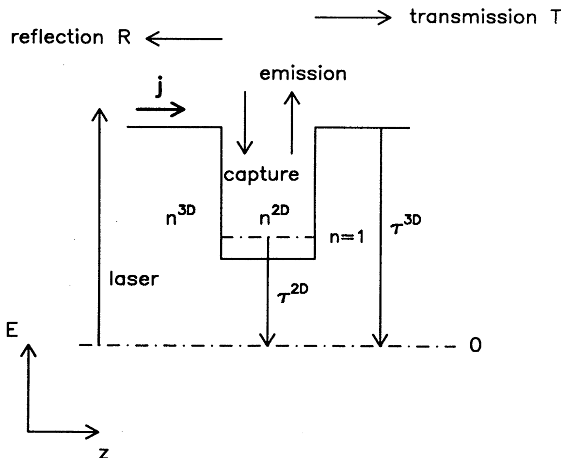

FIG. 11. Schematic picture of the transport processes and variables involved in our model.

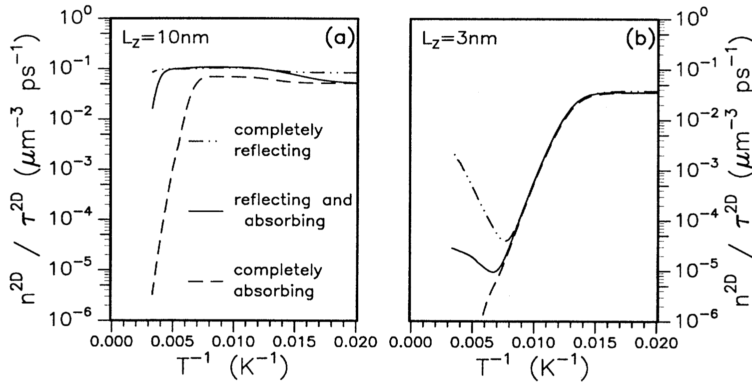

FIG. 12. Simulation of the photoluminescence of a sample of series C ($L_{z1}=3$ nm, $L_{z2}=10$ nm, $L_B=60$ nm) with three different sets of GaAs/$Al_yGa_{1-y}As$ interface parameters. The behavior of the PL intensity (given by n^{2D}/τ^{2D}) of the $L_{z2}=10$ nm quantum well (a) and the $L_{z1}=3$ nm quantum well (b) is depicted in an Arrhenius plot.

about the character of the barrier out of the high-temperature behavior of the quantum-well luminescence.

V. DISCUSSION

To demonstrate the excellent agreement between theory and experiment, we now compare three characteristic sets of measured data (see Sec. II) with the corresponding theoretical results. All simulations are performed using the measured time constants (as described in Sec. III), the calculated capture and emission parameters (Appendix A), and a calculated diffusion coefficient obtained from Ref. 32 which is similar to a measured one reported in Ref. 33. The absorption coefficient is taken from the literature.[34] The free eligible surface parameters are used to fit the experiments.

In Fig. 13 the PL intensity of a sample of series B (including one quantum well with $L_z=3$ nm) is presented. At lower temperatures the dynamics is determined by the capture of particles into the quantum wells and the recombination of these particles inside the wells, causing a PL spectrum dominated by the quantum-well emission. With increasing temperature the carrier density is increasing proportional to the excitonic lifetime (see Appendix B) resulting in a light intensity of the quantum well nearly independent of temperature. The slight decrease of the bulk intensity is caused by a larger diffusion length due to an increasing diffusion coefficient and an increasing exciton lifetime. Hence, more excitons in the bulk reach the well and are absorbed. By further increasing the temperature the emission from the well into the barrier becomes relevant and leads to a decreasing PL intensity of the well and a corresponding increase of the bulk intensity. Above around 160 K, the barrier emission even dominates the PL spectrum. At high temperatures the total luminescence intensity is reduced by nonradiative processes. From our model we conclude that the capture and the subsequent recombination of the excitons by states at the interface to the $Al_yGa_{1-y}As$ barrier is the dominant nonradiative carrier-loss channel in a sample of series B. This is confirmed by the analysis of the total PL intensity of the sample, which starts to decrease at around 100 K, the same temperature where the thermal emission becomes important.

A sample of series C ($L_B=1200$ nm, $L_{z1}=3$ nm, $L_{z2}=10$ nm) is the subject of Fig. 14. The low-temperature behavior is dominated by the already discussed temperature-independent PL intensity. Due to a smaller energy difference to the barrier the narrow well (L_{z1}) is the first one which emits particles and loses inten-

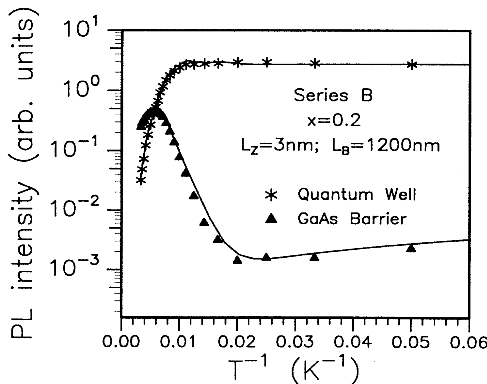

FIG. 13. Comparison between the experiment (symbols) and the theory as described in the text (solid lines) in a sample of series B. The temperature dependence of both, the quantum well and the barrier emission can be fit very well by the theory.

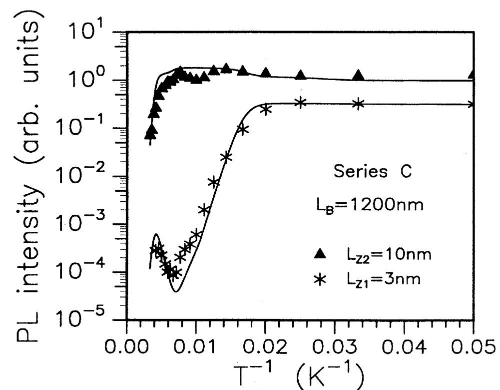

FIG. 14. Temperature dependence of the PL intensity of the shallow ($L_z=3$ nm) and the deep ($L_z=10$ nm) quantum wells of a sample of series C. The hydrodynamic model (solid lines) describes the experiment (symbols) quite good using a GaAs/$Al_yGa_{1-y}As$ interface neither completely absorbing nor completely reflecting.

sity. This is coupled with a raise of the density in the wide wells (L_{z2}). If we compare the 3-nm wells in a sample of series C (Fig. 14) and in a sample of series B (Fig. 13), which both have similar material parameters, we recognize that the starting point of the luminescence decrease depends on the structure (additional $In_xGa_{1-x}As$ layers or not) in the neighborhood of the quantum well under investigation (see also Fig. 6). The characteristic behavior of the exciton dynamics is therefore not only a question of the emission of particles but also of the possibility of the subsequent capture of particles which are reflected from barriers or emitted by other wells. At higher temperatures, we see in Fig. 14 that the decrease of the PL intensity of the wide well is coupled with a reincrease of the narrow well intensity. The discussion of Fig. 12 in Sec. IV tells us that the $Al_yGa_{1-y}As$ barrier of the present sample is neither completely reflecting nor completely absorbing. The reduction of the total PL intensity at higher temperatures due to these nonradiative channels has already been discussed above.

The last figure (Fig. 15) shows the temperature evolution of the Pl intensity of a sample of series A. The curves behave as expected. Depending on the well width and thus on the well depth the quantum wells emit excitons at lower or at higher temperatures. This is characterized by an activation energy depending on the barrier height. The permanent decrease of the intensity in the high-temperature regime shows that the boundaries are absorbing quite strongly what is expected from a free surface and an interface to the substrate. The decrease of the PL intensity is modified by the coupling between the wells via transport in the barrier. At lower temperatures the behavior is rather strange. The PL intensities of the different quantum wells deduced from the experiments differ by about one order of magnitude. However, the diffusion coefficient at these temperatures is so small that each well should capture only the particles in its next neighborhood. Thus, all wells are expected to have similar densities and luminescence intensities.

In our case, the problem was solved by assuming an exciton temperature larger than the lattice temperature. We take an exciton temperature T_{ex}, which is the arithmetic average of the lattice temperature T and a critical temperature T_c (for $T_c = 100$ K, we obtain a good description of the experimental data). This seems to be realistic because due to small-particle densities and a small coupling to acoustic phonons at these low temperatures the particle cooling below the optical phonon limit is slowed down.[35] With a higher thermal energy the excitons, captured by the narrow wells, may leave them again. They are captured finally by the wide wells. Thus we get the desired quotient of the intensities.

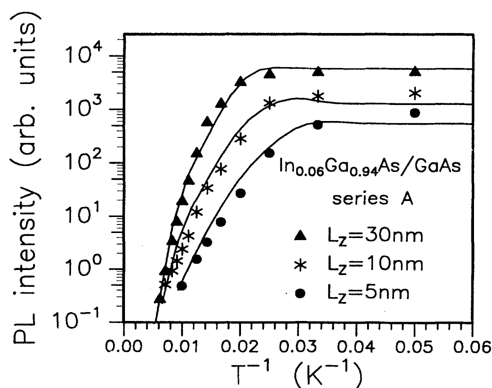

FIG. 15. The PL intensity vs temperature in an Arrhenius plot for a sample of series A. Experiment (symbols) and theory (solid lines) agree very well.

Another possible effect causing a discrepancy between theory and experiment at low temperatures could be the influence of nonlocal carrier capture due to coherence effects. Such a behavior would be important especially at low temperatures, where the coherence length is increased causing a deviation from our hydrodynamic model.

We would like to discuss shortly the limits of validity of our model at high temperatures or high excitation densities, where the influence of electron-hole pairs becomes more and more important. We do not expect a significant change of the activation energy of the thermal emission process in the case of predominantly electron-hole pair recombination with respect to excitonic emission, at least in the density region, where band filling effects can be neglected. This is because of the reason of neutrality, only excitons or electron-hole pairs can leave the quantum well (see the discussion in Sec. II). We have checked this prediction by increasing the ratio between the concentration of electron-hole pairs and excitons by increasing the excitation density of the laser. For negligible band filling effects we have found an activation energy independent of excitation density. On the other hand, the difference between excitons and free electron-hole pairs—concerning the density of states and the Fröhlich interaction with LO phonons as well as the diffusion coefficient in the barrier—possibly modify the onset of the thermal emission with respect to the predictions of our excitonic hydrodynamic model. However, it would be difficult to analyze these deviations quantitatively because of the additional nonradiative process occurring at higher temperatures. For the experiments presented in this paper the excitonic model describes the experimental data very well, because in each case the thermal emission process starts at temperatures, where the collapse of excitons is the dominant recombination channel.

VI. SUMMARY

We have investigated experimentally and theoretically the competition between the carrier capture and the thermal emission in quantum-well heterostructures. Different sets of sample structures are used to demonstrate the importance of the complete sample geometry of these processes. We have found a thermal-activated behavior of the temperature evolution of the PL intensity with an activation energy corresponding to the exciton confinement in the quantum well. The onset of the PL intensity reduction is determined by the whole sample structure (barrier geometry, additional layers, interface quality). Time-resolved experiments are used to extract the characteristic time constants, which are responsible

for the exciton dynamics. While at lower temperatures the radiative excitonic recombination dominates and the measured lifetime is modified at increasing temperature due to the thermal emission. A hydrodynamic model including exciton transport in the barrier, capture, and emission via LO-phonon scattering as well as nonradiative recombination at the heterointerfaces was evaluated to describe our experimental data quantitatively. Using the experimental values for the time constants, we are able to fit the temperature dependence of the PL intensity for the samples investigated very well. The deviation from the Arrhenius behavior due to the coupling of the various quantum wells and interfaces via transport in the barrier can be completely understood in the light of our model.

We would like to emphasize that our results are of great importance for the analysis of time-integrated and time-resolved experiments at higher temperatures especially in shallow quantum wells (small well widths or low barrier heights). For the development of semiconductor heterostructure lasers which should operate at room temperature, it is important to avoid the influence of thermal emission, which could be an efficient carrier-loss mechanism, by using an appropriate sample structure. For analyzing dynamic properties of multi-quantum-well lasers via the rate equation model the present theory is a pronounced improvement with respect to the simple three-level model used up to now, which is only a poor description of the interaction between quantum wells and the barrier.

ACKNOWLEDGMENTS

We would like to express our thanks to T. Kuhn and M. H. Pilkuhn for stimulating discussions, J. Kovac for experimental assistance, and W. Schlapp and R. Lösch for assistance in the sample growth. This work was supported by Deutsche Forschungsgemeinschaft.

APPENDIX A

To get expressions for s_i^c and τ_i^{out} we have first to calculate the eigenstates in the quantum well and above the band edge of the barrier. Formally, a subband number is introduced by mapping the calculated energies on the energies $E=E_0 n^2$ of a quantum well with infinitely high barriers $[E_0=(\hbar\pi/L_z)^2/2m^*]$, where the barrier band-edge energy V_0 separates energy regimes with different density of states. Assuming a Boltzmann distribution and using the transition probability for optical phonon emission and absorption given by Ref. 31 we get

$$s_i^c=\frac{\beta e^2\omega_{\text{LO}}}{32\epsilon_p E_0}(n_{\text{LO}}+1)\int_{n_c}^{\sqrt{n_c^2+\Omega}} dn\frac{n}{\sqrt{n^2-n_c^2}}\exp[-\beta(n^2-n_c^2)]$$
$$\times\sum_{m=m_1}^{n_c}\left[\frac{1}{n-m}\exp[\beta(B_\Omega^-)^2](\Phi\{\sqrt{\beta[(B_\Omega^-)^2+n_c^2-n^2+\Omega]}\}-\Phi(\sqrt{\beta}B_\Omega^-))\right.$$
$$\left.+\frac{1}{n+m}\exp[\beta(B_\Omega^+)^2](\Phi\{\sqrt{\beta[(B_\Omega^+)^2+n_c^2-n^2+\Omega]}\}-\Phi(\sqrt{\beta}B_\Omega^+))\right], \tag{A1}$$

$$\frac{1}{\tau_i^{\text{out}}}=\left[\sum_{m=m_1}^{n_c}[\exp(-\beta m^2)-\exp(-\beta n_c^2)]\right]^{-1}\frac{\beta e^2\omega_{\text{LO}}}{8\epsilon_p E_0 L_z^2}n_{\text{LO}}$$
$$\times\sum_{m=m_1}^{n_c}\int_{n_c^2-m^2-\Omega}^{n_c^2-m^2}d\varepsilon\exp[-\beta(m^2+\varepsilon)]\int_{n_c}^{\sqrt{\varepsilon+\Omega}}dn\frac{n}{\sqrt{n^2-n_c^2}}$$
$$\times(\{[2m(m-n)+\Omega]^2+4(m-n)^2\varepsilon\}^{-1}$$
$$+\{[2m(m+n)+\Omega]^2+4(m+n)^2\varepsilon\}^{-1}). \tag{A2}$$

We used the abbreviations $\beta=E_0/k_BT$, $n_c^2=V_0/E_0$, $\Omega=\hbar\omega_{\text{LO}}/E_0$, and

$$B_\Omega^\pm(n,m)=\frac{2n(n\pm m)-\Omega}{2(n\pm m)}, \tag{A3}$$

$$\frac{1}{\epsilon_p}=\frac{1}{4\pi\epsilon_0}\left[\frac{1}{\epsilon_r(\infty)}-\frac{1}{\epsilon_r(0)}\right]. \tag{A4}$$

ω_{LO} is the frequency of the longitudinal-optical phonons, n_{LO} their distribution function, ε_r the dielectric functions, Φ the error function, n the number of states above the band edge, m the number of states below, and m_1 the formal number of the lowest subband.

APPENDIX B

Using the steady-state form of the equation system and the boundary conditions we get as formal solution of the

density in a quantum well

$$n_i^{2D} = \frac{g_i^{2D} e^{-\alpha_i^{2D} z_i} + (n^{3D}|_i^l + n^{3D}|_i^r) s_i^c}{1/\tau_i^{out} + 1/\tau_i^{2D}} . \quad \text{(B1)}$$

We recognize that n_i^{2D} is proportional to τ_i^{2D} for low temperatures, when $1/\tau_i^{out}$ is negligible. For the density in parts of the bulk between the wells we make the ansatz

$$n^{3D} = \frac{g^{3D} e^{-\alpha^{3D} z}}{1/\tau^{3D} - D(\alpha^{3D})^2} + A_{2i-1} e^{z/\sqrt{D\tau^{3D}}} + A_{2i} e^{-z/\sqrt{D\tau^{3D}}} , \quad z \in (z_{i-1}, z_i) . \quad \text{(B2)}$$

The coefficients A_i are easily obtained by solving a matrix equation.

---

[1]W. Rideout, W. F. Sharfin, E. S. Koteles, M. O. Vassell, and B. Elman, IEEE Photon. Technol. Lett. **3**, 784 (1991).

[2]E. H. Reihlen, A. Persson, T. Y. Wang, K. L. Fry, and G. B. Stringfellow, J. Appl. Phys. **66**, 5554 (1989).

[3]J. Y. Tang, K. Hess, N. Holonyak, Jr., J. J. Coleman, and P. D. Dapkus, J. Appl. Phys. **53**, 6043 (1982).

[4]N. Ogasawara, A. Fujiwara, N. Ohgushi, S. Fukatsu, Y. Shiraki, Y. Katayama, and R. Ito, Phys. Rev. B **42**, 9562 (1990).

[5]H.-J. Polland, K. Leo, K. Rother, K. Ploog, J. Feldmann, G. Peter, E. O. Göbel, K. Fujiwara, T. Nakayama, and Y. Ohta, Phys. Rev. B **38**, 7635 (1988).

[6]H. Hillmer, A. Forchel, T. Kuhn, G. Mahler, and H. P. Meier, Phys. Rev. B **43**, 13992 (1991).

[7]U. Cebulla, G. Bacher, A. Forchel, D. Schmitz, H. Jürgensen, and M. Razeghi, Appl. Phys. Lett. **55**, 933 (1989).

[8]B. Deveaud, F. Clérot, A. Regreny, K. Fujiwara, K. Mitsunaga, and J. Ohta, Appl. Phys. Lett. **55**, 2646 (1989).

[9]B. Deveaud, J. Shah, T. C. Damen, and W. T. Tsang, Appl. Phys. Lett. **52**, 1886 (1988).

[10]R. Kersting, X. Q. Zhou, K. Wolter, D. Grützmacher, and H. Kurz, Superlatt. Microstruct. **7**, 345 (1990).

[11]D. Y. Oberli, J. Shah, J. L. Jewell, T. C. Damen, and N. Chand, Appl. Phys. Lett. **54**, 1028 (1989).

[12]S. Morin, B. Deveaud, F. Clérot, A. Regreny, K. Fujiwara, K. Mitsunaga, and J. Ohta, Superlatt. Microstruct. **8**, 77 (1990).

[13]J. A. Brum and G. Bastard, Phys. Rev. B **33**, 1420 (1986).

[14]T. Kuhn and G. Mahler, Solid State Electron. **32**, 1851 (1989).

[15]J. A. Brum, T. Weil, J. Nagle, and B. Vinter, Phys. Rev. B **34**, 2381 (1986).

[16]A. Weller, P. Thomas, J. Feldmann, G. Peter, and E. O. Göbel, Appl. Phys. A **48**, 509 (1989).

[17]S. V. Kozyrev and A. YA. Shik, Fiz. Tekh. Poluprovodn. **22**, 105 (1988) [Sov. Phys. Semicond. **22**, 64 (1988)].

[18]P. W. M. Blom, J. E. M. Haverkort, and J. H. Wolter, Appl. Phys. Lett. **58**, 2767 (1991).

[19]Yoshimasa Murayama, Phys. Rev. B **34**, 2500 (1986).

[20]G. Bacher, H. Schweizer, J. Kovac, A. Forchel, H. Nickel, W. Schlapp, and R. Lösch, Phys. Rev. B **43**, 9312 (1991).

[21]J. Feldmann, K. W. Goossen, D. A. B. Miller, A. M. Fox, J. E. Cunningham, and W. Y. Jan, Appl. Phys. Lett. **59**, 66 (1991).

[22]J. D. Lambkin, D. J. Dunstan, K. P. Homewood, L. K. Howard, and M. T. Emeny, Appl. Phys. Lett. **57**, 1986 (1990).

[23]P. Michler, A. Hangleiter, M. Moser, M. Geiger, and F. Scholz, Phys. Rev. B **46**, 7280 (1992).

[24]Craig S. Lent, Lie Liang, and Wolfgang Porod, Appl. Phys. Lett. **54**, 2315 (1989).

[25]H. Nickel, R. Lösch, W. Schlapp, H. Leier, and A. Forchel, Surf. Sci. **228**, 340 (1990).

[26]Note that the thickness of the quantum well is only 3 nm compared to the total GaAs barrier thickness of 2400 nm. For that reason, the GaAs signal for an excitation below the GaAs barrier is more than two orders of magnitude smaller than for an excitation above the barrier.

[27]B. K. Ridley, Phys. Rev. B **41**, 12 190, (1990).

[28]J. Feldmann, G. Peter, E. O. Göbel, P. Dawson, K. Moore, C. Foxon, and R. J. Elliott, Phys. Rev. Lett. **59**, 2337 (1987).

[29]M. Gurioli, A. Vinattieri, M. Colocci, C. Deparis, J. Massies, G. Neu, A. Bosacchi, and S. Franchi, Phys. Rev. B **44**, 3115 (1991).

[30]T. Kuhn and G. Mahler, Phys. Scr. **38**, 216 (1988).

[31]B. K. Ridley, J. Phys. C **15**, 5899 (1982).

[32]T. Held, T. Kuhn, and G. Mahler, Phys. Rev. B **41**, 5144 (1990).

[33]H. Hillmer, A. Forchel, S. Hansmann, M. Morohashi, E. Lopez, H. P. Meier, and K. Ploog, Phys. Rev. B **39**, 10 901 (1989).

[34]M. D. Sturge, Phys. Rev. **127**, 768 (1962).

[35]P. K. Basu and Partha Ray, Phys. Rev. B **45**, 1907 (1992).